Macromolecular Research, Vol. 23, No. 2, pp 149-155 (2015)
DOI 10.1007/s13233-015-3032-2

www.springer.com/13233
pISSN 1598-5032 eISSN 2092-7673

PAN Electrospun Nanofibers Reinforced with Ag_2CO_3 Nanoparticles: Highly Efficient Visible Light Photocatalyst for Photodegradation of Organic Contaminants in Waste Water

Gopal Panthi[1], Mira Park[1], Soo-Jin Park*[,2], and Hak-Yong Kim*[,1]

[1]*Department of Organic Materials and Fiber Engineering, Chonbuk National University, Jeonbuk 561-756, Korea*
[2]*Department of Chemistry, Inha University, Nam-gu, Incheon 402-751, Korea*

Received July 22, 2014; Revised November 18, 2014; Accepted December 7, 2014

Abstract: This paper presents fabrication of polyacrylonitrile (PAN) electrospun nanofibers (NFs) reinforced with Ag_2CO_3 nanoparticles (NPs) as highly efficient visible light photocatalyst. Preparation of the introduced NFs was accomplished by using simple, effective, high yield, and low cost process; electrospinning of Ag_2CO_3/PAN colloidal solution at different applied electric voltages. Photocatalytic efficiency of the introduced nanofiber mats was investigated by photodegradation of three dyes (Methyl orange, Methylene blue, and RhodamineB) under visible light irradiation. Experimental results indicated that the nanofiber mat obtained at applied electric voltage of 18 kV could show higher performance towards the photodegradation of organic contaminants. Moreover, field emission scanning electron microscopy (FE-SEM) and transmission electron microscope (TEM) analysis confirmed the confinement of Ag_2CO_3 NPs inside polymeric NFs, which can overcome the serious problems of photocorrosion of photocatalyst and secondary pollution. Overall, the introduced NFs can be used as efficient, low cost, and healthily safe visible light driven photocatalyst in the field of water treatment and can promote its industrial application, especially in the open water surfaces.

Keywords: electrospinning, photocatalyst, visible light, silver carbonate, organic contaminants.

Introduction

Over the past years, semiconductor photocatalysts have been attracting considerable attention because of their potential applications involving utilization of solar energy[1,2] for the photodegradation of organic contaminants.[3,4] Among the various photocatalysts, titanium dioxide (TiO_2) and zinc oxide (ZnO) are the most widely used photocatalyst materials because of their high photocatalytic efficiency, good stability, low cost, environmental friendliness, and non toxicity.[5,6] However, the wide band gap of TiO_2 (3.2 eV) and ZnO (3.37 eV) limits their photocatalytic performances only in presence of high energy UV-light resulting in a low efficiency in the utilization of solar/visible light. In order to overcome this problem, some remarkable progress has been made in recent years for exploration and fabrication of novel active semiconductor photocatalyst with a band gap corresponding to the energy of visible light, which remain promising for the practical application. Recently, a new photocatalyst silver carbonate (Ag_2CO_3), with narrow band gap of 2.3 eV has been studied as a novel photocatalyst that can exhibit excellent photocatalytic performances towards the photodegradation of organic contaminants under visible light irradiation.[3,7] However, Ag_2CO_3 greatly suffers from poor stability owing to the photocorrosion, which causes the serious deactivation.[8,9] Therefore, various attempts have been made to enhance the stability and photochemical reactivity of Ag_2CO_3 either by synthesizing composite with graphene oxide (GO)[10,11] or by combining with other inorganic materials to develop hetro-structures such as Ag_2O/Ag_2CO_3,[12] Ag_2CO_3/TiO_2,[13] Ag_2CO_3/AgX,[14] Ag_2CO_3/Ag-Ti_5NbO_{14}[15] but the effects on photocatalytic activity of Ag_2CO_3, when a polymer is applied as template to confine the Ag_2CO_3 particles have been rarely studied. Some studies revealed that, when a polymer is applied as templates or co-photocatalyst, not only it confines the semiconductor nanoparticles (NPs) but also protects from photocorrosion and makes the separation process of utilized photocatalyst more convenient.[16] Therefore, selection of suitable polymer is most important to develop polymer-semiconductor composites so that it can show the potential for serving as photocatalyst for the decomposition of organic contaminants under visible light irradiation.[17]

Various methods have been adopted to prepare polymer-semiconductor composites with different sizes and morphol-

*Corresponding Authors. E-mails: khy@chonbuk.ac.kr or sjpark@inha.ac.kr

ogies, which have wide range of applications in photocatalysis, electronics, and optics.[16-18] In this regard, electrospinning has been proven as a novel and efficient process for the fabrication of polymer-semiconductor composite nanofibers (NFs) by incorporating various nanomaterials into polymer matrices. The electrospun nanofibers (ENFs) have unique properties like small diameter, high aspect ratio, large specific surface area, high flexibility for chemical/physical surface functionalization, and unique physicochemical properties.[19-21] Moreover, the morphological structure of ENFs depends on various electrospinning parameters like molecular weight of polymer, flow rate, tip to collector distance, applied electric voltage *etc*.[22]

Hence, this communication demonstrates fabrication of polyacrylonitrile (PAN) ENFs reinforced with Ag_2CO_3 NPs *via* simple, low cost, and high yield process; electrospinning of PAN/Ag_3CO_3 colloidal solution at different applied electric voltages. The morphology of NFs obtained at different applied voltages and their photocatalytic performances towards the photodegradation of organic contaminants in presence of visible light were explored. PAN was chosen for this study due to its advantages over other polymers, such as its easy straightforward synthesis, high environmental stability, and good processibility. More significantly, PAN based ENFs can be easily separated from solution by filtration due to its hydrophobic property and low density.[23]

Experimental

Materials. The materials used in this study were polyacrylonitrile (PAN, MW 150,000, Sigma-Aldrich, USA), *N*,*N*-dimethylformamide (DMF, Daejung Chemicals, Korea), Silver nitrate ($AgNO_3$, Sigma-Aldrich, USA), Ammonia solution (extra pure grade, Duksan pure chemicals, South Korea), Sodium bicarbonate ($NaHCO_3$, Sigma-Aldrich, USA), Triton X-100 (Sigma-Aldrich, USA), Methyl orange (MO, Sigma-Aldrich, USA), Methylene blue (MB, Sigma-Aldrich, USA), and Rhodamine B (RhB, Sigma-Aldrich, USA). All the chemicals were used as received.

Synthesis of Ag_2CO_3 Nanoparticles. The Ag_2CO_3 nanoparticles were prepare by a simple precipitation reaction between Ag $(NH_3)_2^+$ and $NaHCO_3$.[10] In a typical procedure, 20 mL of ammonia solution was added in drop wise manner to 20 mL of $AgNO_3$ (0.1 M) with constant stirring to form a transparent solution. Then 20 mL of $NaHCO_3$ (0.05 M) was added to the above silver ammonia mixture solution with a rate of 0.5 mL min^{-1} under constant stirring. The product obtained was centrifuged and washed many times with deionized water and ethanol and finally dried under vacuum at 30 ºC for 5 h.

Fabrication of PAN Electrospun NFs Reinforced with Ag_2CO_3. First of all, Ag_2CO_3 NPs were ultrasonicated in DMF for 2 h. Then, Triton X-100 (with the same weight of Ag_2CO_3) was added to the solution and ultrasonicated for another 2 h. Triton X-100 was used in this experiment as surfactant to aid in the proper dispersion of Ag_2CO_3 NPs. In the final step, an appropriate amount of PAN was added to the previously prepared Ag_2CO_3/Triton X-100/DMF mixture solution to get a PAN solution of 10 wt% and the final solution (mass ratio of PAN:Ag_2CO_3=5:3) was ultrasonicated for another 1 h. Subsequently, the final solution was loaded in a plastic syringe equipped with metallic needle connected to a high voltage power supply (high voltage power supply, HV 30/ESN-HV30N, Nano NC, Korea) capable to produce DC voltages from 0 to 30 kV and electrospun at different applied electric voltages with a constant flow rate of 1 mL/h through a syringe pump. The developing NFs were collected on aluminum foil wrapped over rotating drum collector at 15 cm apart from needle tip. All experiments were conducted at room temperature and atmosphere pressure. The schematic illustration for the fabrication of PAN electrospun NFs reinforced with Ag_2CO_3 NPs is given in Figure 1. Thus obtained NFs mats were vacuum dried at 70 ºC for 12 h in order to remove the residual solvent. For the convenience of description, the NFs mats obtained at different applied voltages were herein tagged as; PAN/Ag_2CO_3-14, PAN/Ag_2CO_3-18, and PAN/Ag_2CO_3-22 corresponding to nanofiber mats obtained at 14, 18, and 22 kV, respectively.

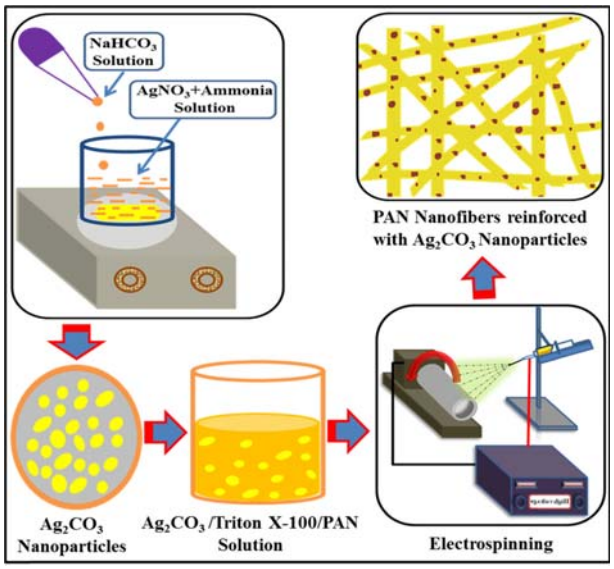

Figure 1. Schematic illustration for the fabrication of PAN electrospun NFs reinforced with Ag_2CO_3 nanoparticles.

Characterization. The morphologies of PAN/Ag_2CO_3 nanofiber mats were observed by field emission scanning electron microscopy (FE-SEM, S-7400, Hitachi, Japan) and the elemental composition was checked using energy dispersive spectrometer (EDS). The particle size and distribution were examined using a transmission electron microscope (TEM, Model JEM-2100 F, JEOL, Co.) with a 200 kV accelerating voltage. The samples were prepared by directly collecting the nanofibers on TEM grid during electrospinning. The phase and crystallinity of the NPs were obtained with a Bruker X-ray diffractometer (XRD, BRUCKER D2 PHASER, Germany) with CuK_α

(λ=1.540 Å) radiation over Bragg angles ranging from 10° to 70°. Fourier transform infrared (FTIR) spectroscopy was performed to characterize the bonding configurations of polymer with semiconductor NPs (FT/IR-4200; Jasco International Co., Ltd.). The elemental analysis was conducted using X-ray photoelectron spectroscopy (XPS, VG scientific Co., ESCA LAB MK II) to determine the elemental composition of the PAN/Ag_2CO_3 nanofiber mat. UV-vis diffuse reflectance spectra (DRS) were measured using a UV-vis spectrophotometer (Lambda 900, PerkinElmer, USA). UV absorbance was measured by UV-vis spectrophotometer (S-3100 SCINCO CO., LTD., Korea).

Photocatalytic Activity Investigation. The photocatalytic activity of the samples (0.2 g, the mass ratio of PAN: Ag_2CO_3 =5:3) were investigated by observing the degradation of aqueous solution of MO, MB, and RhB dyes (50 mL, 10 ppm concentration) in a simple photochemical reactor. Prior to irradiation, the suspensions were magnetically stirred for 10 min under dark condition to established adsorption/desorption equilibrium between dyes and photocatalyst. In this investigation, the reactions were carried out in inverted glass bottles under simulated solar light irradiation. The visible light (λ > 420 nm) was obtained by a 500 W xenon lamp with a glass cutoff filter (ABET Technology, USA) to completely remove any radiation below 420 nm. At the regular interval of time, a 2 mL of aliquots were taken out and the concentration of the dye was measured by recording the UV absorbance using a UV-vis spectrophotometer.

Results and Discussion

Figure 2 shows the FESEM images and FESEM-EDX of PAN/Ag_2CO_3 nanofiber mats obtained at different applied electric voltages (PAN/Ag_2CO_3-14, PAN/Ag_2CO_3-18, and PAN/Ag_2CO_3-22). It was also observed that when the applied electric voltage was decreased from 14 to 10 kV, formation of NFs did not occur because the electrostatic force could not overcome the surface tension of polymer solution. As shown in figure, all formulations possessed continuous and smooth NFs with random orientation due to bending instability accompanied with spinning jet. Interestingly, the Ag_2CO_3 NPs weren't observed on the surface of PAN NFs, which indicated that the NPs were confined inside the polymeric NFs. However, it was observed that the diameter of NFs decreased with the increase of applied electric voltage from 14 to 22 kV. As the result, the average diameter of NFs was found to be 470, 390, and 350 nm for PAN/Ag_2CO_3-14 (Figure 2(a)), PAN/Ag_2CO_3-18 (Figure 2(b)), and PAN/Ag_2CO_3-22 (Figure 2(c)) nanofiber mats, respectively. The decrease in average diameter of NFs can be explained in terms of increase in applied electric voltage, which induces more charges on the solution surface and fully stretch the solution jet to yield uniform, smooth, and thinner NFs.[24-26] Moreover, the EDS analysis of PAN/Ag_2CO_3 nanofiber mat (Figure 2(d)) revealed, the presence of considerable amount of C, Ag, and O elements, which further confirmed that the obtained nanofiber mat was composed of both Ag_2CO_3 and PAN.

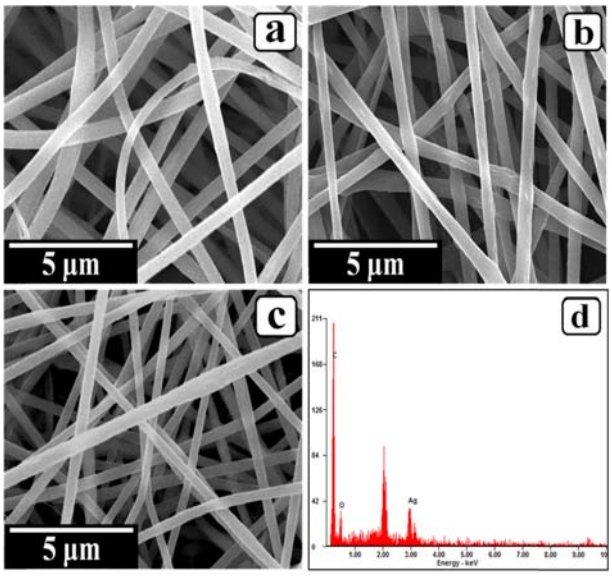

Figure 2. FE-SEM images of (a) PAN/Ag_2CO_3-14, (b) PAN/Ag_2CO_3-18, (c) PAN/Ag_2CO_3-22 nanofiber mat, and (d) FE-SEM-EDX of PAN/Ag_2CO_3 nanofiber mats.

Figure 3 represents the XRD patterns of Ag_2CO_3 powder and PAN/Ag_2CO_3 nanofiber mats obtained at different applied electric voltages. The diffraction peaks in all formulations can be indexed to the monoclinic phase of crystalline Ag_2CO_3 (JCPDS no. 26-0339).[12] However, the relative intensities Ag_2CO_3 NPs diffraction peaks were reduced in PAN/Ag_2CO_3 nanofiber mats (Figure 3(b)-(d)) compared with bare Ag_2CO_3 NPs, which should be ascribed to the tiny proportion of Ag_2CO_3 NPs encapsulated in PAN NFs. No peaks from other impurities like metallic Ag were observed, suggesting that only Ag_2CO_3 NPs were present in the PAN electrospun nanofiber mats.

To observe the more detail morphological characteristics

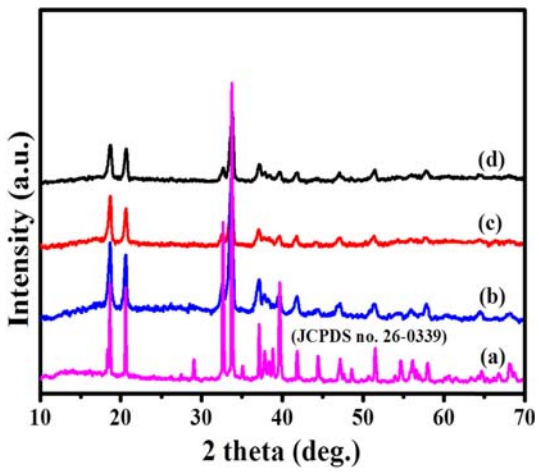

Figure 3. XRD patterns of (a) Ag_2CO_3 powder, (b) PAN/Ag_2O_3-14, (c) PAN/Ag_2CO_3-18, and (d) PAN/Ag_2CO_3-22 nanofiber mat.

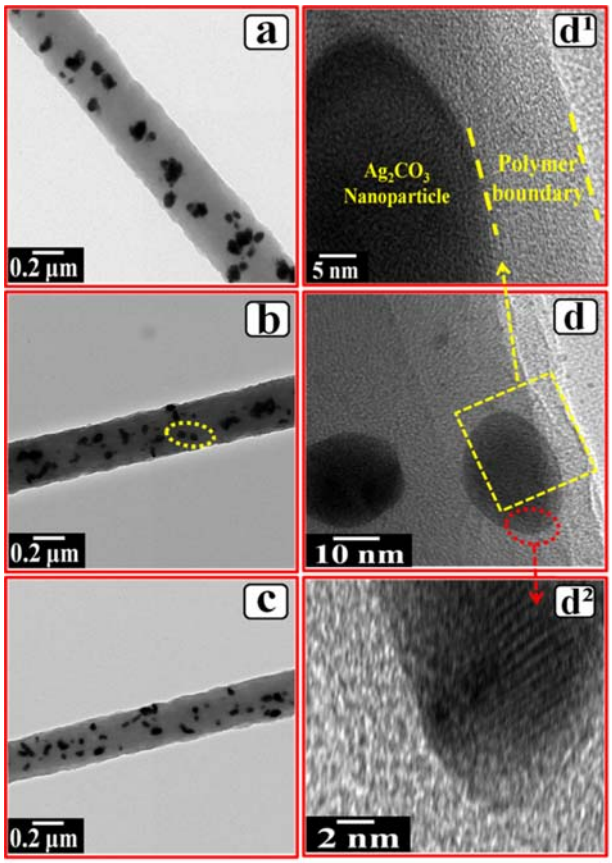

Figure 4. TEM images of (a) PAN/Ag_2CO_3-14, (b) PAN/Ag_2O_3-18, and (c) PAN/Ag_2CO_3-22 nanofiber mat, and (d) high magnification TEM image of yellow circled area for (b). Panel (d^1) and (d^2) represent the HR-TEM images of yellow and red circled area for (d), respectively.

of PAN/Ag_2CO_3 nanofiber mats, dispersion of Ag_2CO_3 NPs inside PAN NFs and their crystallinity, TEM/HR-TEM studies were conducted (Figure 4). As shown in figure, in all formulations, the NPs appeared slightly aggregated but dispersed relatively homogeneously inside the NFs. An important observation from the TEM analysis of these nanofiber mats was that the degree of dispersion of NPs inside the NFs was found to be increased with the increase of applied electric voltage from 14-22 kV (Figure 4(a)-(c)). Here, we consider that the higher degree of dispersion of Ag_2CO_3 NPs is associated with electrostatic repulsion. Because the NPs experience more charges with the increase in applied voltage and result in an increased electrostatic repulsion with each other, which favors the NPs for higher degree of dispersion. Moreover, as shown in the high magnified TEM image (yellow-marked area in Figure 4(b)), NPs are sheathed by the polymer boundary (Figure 4(d), (d^1)), which can protect the NPs from corrosion and agglomeration. Also, the perfectly crystalline structure of Ag_2CO_3 NPs (red-marked area in Figure 4(d)) was clearly visible in HR-TEM image (Figure 4(d^2)). As shown in the figure, the parallel atomic

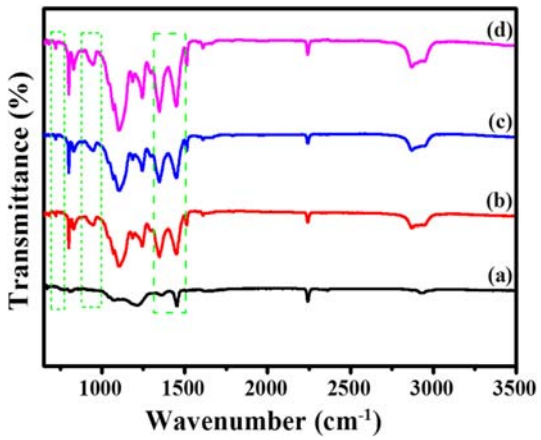

Figure 5. FTIR spectra of (a) pure PAN, (b) PAN/Ag_2CO_3-14, (c) PAN/Ag_2CO_3-18, and (d) PAN/Ag_2CO_3-22 nanofiber mat.

planes can reveal the excellent crystallinity of the prepared NPs.

The FTIR spectra of pure PAN and PAN/Ag_2CO_3 nanofiber mats are shown in Figure 5. The characteristic absorption peaks at around 2242 cm^{-1} are assigned to the (CN) nitrile group of PAN, besides, a series of characteristic bands obtained in the regions 1220-1270, 1350-1380, 1450-1460, and 2870-2931 cm^{-1}, are assigned to the aliphatic CH group vibrations of different modes in methylene group of PAN.[27] In comparison to pure PAN, the FTIR spectra of PAN/Ag_2CO_3 nanofiber mats (Figure 5(b)-(d)), the absorption bands obtained at around 705, 896, 1382, and 1451 cm^{-1} are attributed to CO_3^{2-} in Ag_2CO_3.[11] Furthermore, a shift of the -CN- bond vibration was not detected in all formulations indicating that there was no any bond formation between -CN- group in PAN and Ag_2CO_3 NPs. So, it could be concluded that Ag_2CO_3 NPs were solely physically embedded in the PAN nanofiber mats.

In order to analyze the chemical state of elements in PAN/Ag_2CO_3 nanofiber mat, XPS analysis was carried out (Figure 6). The XPS spectra for C1s, N1s, Ag3d, and O1s are shown in the survey spectrum (Figure 6(a)). Also, information regarding the specific nature of C, Ag, and O elements is obtained from high resolution XPS spectra. The high resolution spectrum of C1s (Figure 6(b)) contains two distinct peaks at about 284.5 and 286.6 eV corresponding to C-C and C-O groups, respectively.[10] Figure 6(c) displays high resolution XPS spectrum of Ag3d, two individual peaks at about 368.2 and 374.2 eV can be assigned to the $Ag3d_{5/2}$ and $Ag3d_{3/2}$ states indicating the presence of Ag^+.[28] Similarly, the peak at about 531 eV in the high resolution spectrum (Figure 6(d)) belongs to the O1s state of Ag_2CO_3.[29] Moreover, the XPS spectra of N1s obtained at about 396 eV in the survey spectrum (Figure 6(a)), confirms the presence of N element in PAN polymer. Furthermore, to elucidate the change of chemical state of PAN/Ag_2CO_3 nanofiber mat after use, XPS measurement was performed for PAN/Ag_2CO_3-18 nanofiber mat obtained after photodegradation of RhB solution (Figure 6(a), inset). As shown in the

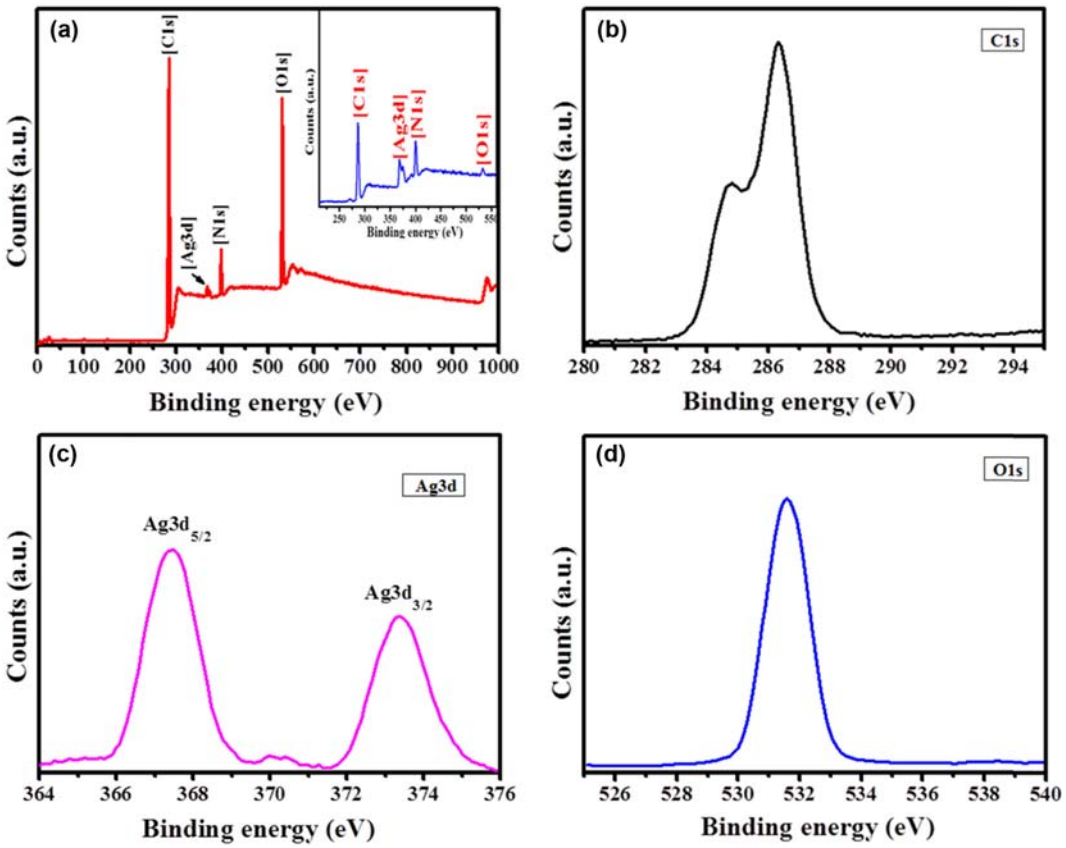

Figure 6. XPS spectra of PAN/Ag_2CO_3-18 nanofiber mat; (a) survey spectrum, and high resolution XPS spectra for (b) C1s, (c) Ag3d, and (d) O1s (Inset; survey spectrum of PAN/Ag_2CO_3-18 nanofiber mat obtained after photodegradation of RhB solution).

figure, Ag, C, N, and O elements were present in the used nanofiber mat without any significant change on the composition. Therefore, from all these observations it can be concluded that the proposed preparation technique did not introduce any impurities in the nanofiber mat.

The optical absorption properties of a photocatalyst play an important role in determining its catalytic performance. Therefore, UV-vis diffuse reflectance spectra of Ag_2CO_3 powder and PAN/Ag_2CO_3 -18 nanofiber mat were examined and results are shown in Figure 7. It is clearly seen that the Ag_2CO_3 powder has an absorption edge around 480 nm (Figure 7(a)) and exhibit strong absorption in the visible ranges as reported earlier.[7] Regarding the PAN/ Ag_2CO_3 -18 nanofiber mat, similar absorption ranges to the Ag_2CO_3 powder were observed. But the absorption intensity was found to be slightly increased (Figure 7(b)). This feature suggested that the visible light absorption properties of Ag_2CO_3 powder could be further enhanced by incorporating within PAN polymer.

Figure 8(a) shows the photocatalytic performances of different samples towards the photodegradation of MO, MB, and RhB dye solutions under visible light irradiation. In order to evaluate the absorption property of pristine PAN nanofiber mat towards all three dye solutions, experiments were carried out

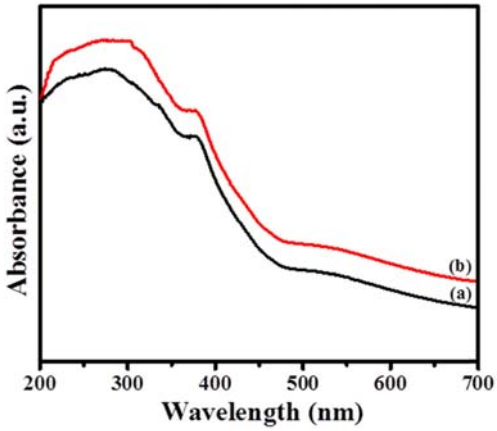

Figure 7. UV-vis diffuse reflectance spectra of (a) Ag_2CO_3 powder and (b) PAN/Ag_2CO_3 -18 nanofiber mat.

under similar condition using PAN nanofiber mat alone and found to be negligible. The degradation is represented as the variation of (C/C_0) with irradiation time, where C_0 and C are the concentrations of dye solutions at the initial time and at time t, respectively. From the results, it is clear that the complete degradation of MO, MB, and RhB occurred within 30, 35,

and 50 min, respectively in case of utilizing PAN/Ag_2CO_3-18 nanofiber mat, while PAN/Ag_2CO_3-22 and PAN/Ag_2CO_3-14 nanofiber mats required (35 and 40 min), (40 and 45 min), and (60 and 70 min) for the same purpose. Additionally, the pure Ag_2CO_3 powder could degrade MO, MB, and RhB, dyes in 43, 55, and 78 min, respectively, which may be due to the low solubility and photocorrosion of Ag_2CO_3.[30] Therefore, we believe that, in the composite nanofiber mats, Ag_2CO_3 NPs were encapsulated in the NFs, and PAN could protect the photocatalyst from dissolution and photocorrosion. Here, we suppose the higher photocatalytic efficiency of PAN/Ag_2CO_3-18 nanofiber mat is due to appropriate dispersion of NPs in the PAN NFs, while in case of PAN/Ag_2CO_3-14 nanofiber mat, the diameter of NFs is larger and the NPs are dispersed throughout the NFs with slight agglomeration compared with PAN/Ag_2CO_3-18 nanofiber mat, which caused the decrease in effective surface area of NPs leading to the lesser photocatalytic efficiency. Similarly, in the case of PAN/Ag_2CO_3-22 nanofiber mat, although the diameter of fiber is smaller, the dispersion of NPs is higher compared with PAN/Ag_2CO_3-18 nanofiber mat. Therefore, the no. of NPs per unit area of NFs decreased, which caused ultimate decrease in photocatalytic efficiency. However, the higher photocatalytic efficiency of PAN/Ag_2CO_3-18 nanofiber mat needs more detail study. The absorbance variations of MO, MB, and RhB solutions utilizing of PAN/Ag_2CO_3-18 nanofiber mat under visible light at different irradiation time are shown in Figure 8(b). The absorbance peaks corresponding to MO at 464 nm, MB at 665 nm, and RhB at 554 nm are diminished gradually with the increase in irradiation time. However, in this work, maximum absorption wave lengths of MO, MB, and RhB were not shifted, which indicated that benzene/heterocyclic rings were decomposed rather than the simple decoloration process.[31,32]

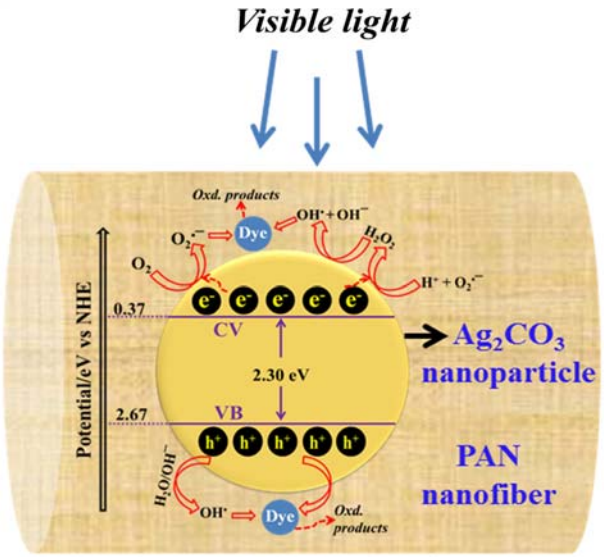

Figure 9. Conceptual illustration for the photodegradation of organic pollutants using proposed PAN/Ag_2CO_3 nanofiber mat.

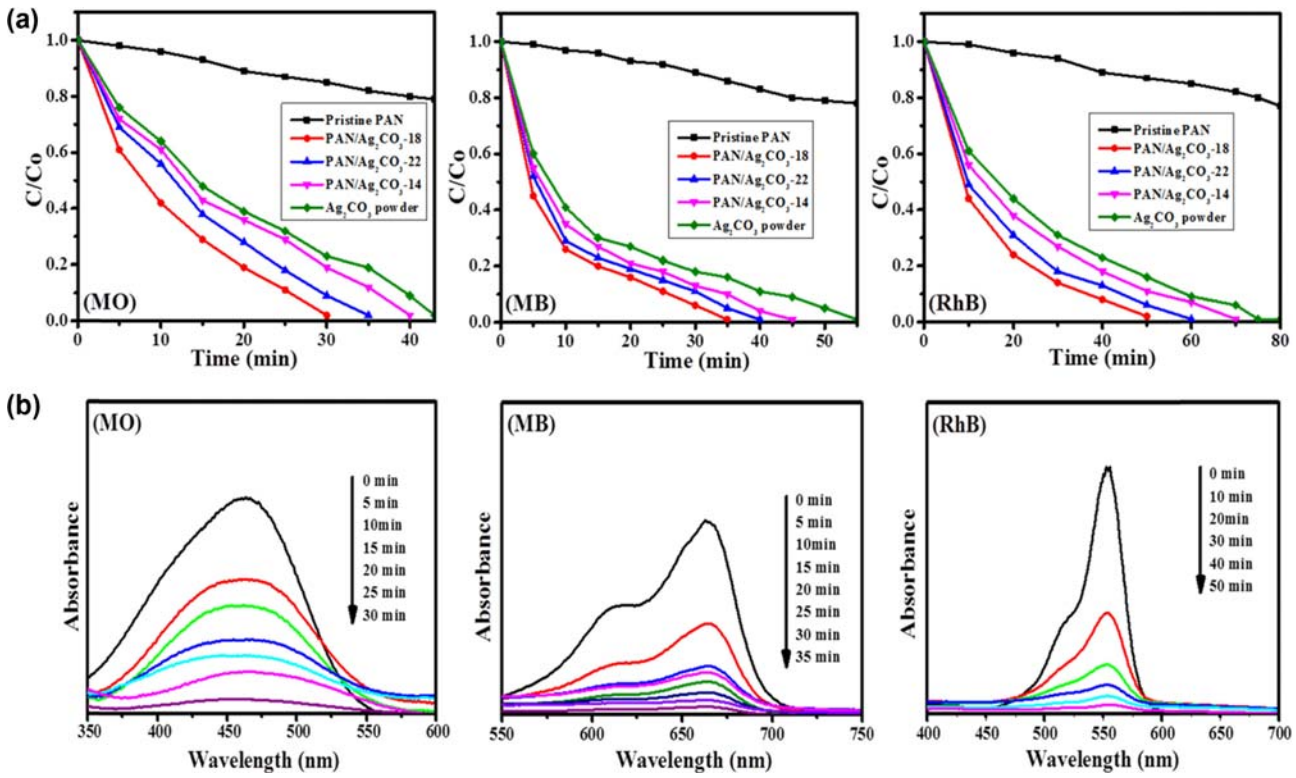

Figure 8. (a) Photocatalytic performances of Pristine PAN, PAN/Ag_2CO_3-18, PAN/Ag_2CO_3-22, PAN/Ag_2CO_3-14 nanofiber mats, and Ag_2CO_3 powder. (b) Absorbance variations of MO, MB, and RhB solutions utilizing of PAN/Ag_2CO_3-18 nanofiber mat.

The proposed mechanism of photocatalytic activity of Ag_2CO_3 NPs has been introduced in Figure 9, which shows a conceptual illustration for the photodegradation process of organic contaminants using PAN/Ag_2CO_3 nanofiber mat. Low recombination between the excited electrons and holes is the significant characteristic of the Ag_2CO_3 to achieve good photocatalytic activity. Briefly, at the beginning, visible light leads to excite the electrons from the valence band to the conduction band leaving behind holes. Where photogenerated electrons are captured by dissolved O_2 in dyes solutions to produce $O_2^{\bullet-}$ radicals. Thus obtained $O_2^{\bullet-}$ radicals can directly oxidize dye molecules or react with H^+ to produce H_2O_2 leading to the formation of $OH^\bullet$ radicals, responsible for the oxidation of dyes. At the same time, photogenerated holes either directly oxidize dye molecules or react with H_2O and OH^- ions generating $OH^\bullet$ radicals to oxidize dyes.

The possible photochemical reactions taking place can be summarized as follows:

$$Ag_2CO_3 \xrightarrow{h\nu} \underset{\text{(Valence band)}}{h^+} + \underset{\text{(Conduction band)}}{e^-}$$

At the conduction band:

$$O_2 + e^- \rightarrow O_2^{\bullet-}$$

$$O_2^{\bullet-} + 2H^+ + e^- \rightarrow H_2O_2$$

$$H_2O_2 + e^- \rightarrow OH^\bullet + OH^-$$

At the valence band:

$$OH^- + h^+ \rightarrow OH^\bullet$$

$$H_2O + h^+ \rightarrow OH^\bullet + H^+$$

Degradation reaction:

$$O_2^{\bullet-}/h^+/OH^\bullet + \text{Organic contaminants} \rightarrow \text{Oxidized products } (CO_2 + H_2O)$$

Conclusions

In summary, PAN electrospun NFs reinforced with Ag_2CO_3 NPs as visible light driven photocatalyst have been successfully fabricated by using a simple and versatile electrospinning process. FESEM and TEM analysis demonstrates that the Ag_2CO_3 NPs were confined inside PAN NFs. The experimental results demonstrated that the applied electric voltage has significant effects on the fiber morphology and photocatalytic performances of as synthesized nanofiber mats. Furthermore, studies of photocatalytic performances indicated that the PAN composite NFs fabricated at applied electric voltage of 18 kV (PAN/Ag_2CO_3-18 nanofiber mat) could show highest photocatalytic activity. Finally, we believe that this strategy can be a new paradigm to fabricate other semiconductor-polymer composite NFs for photocatalytic applications under visible light irradiation.

Acknowledgments. This work was supported by the National Research Foundation of Korea (NRF) grant funded by the Korea Government (MEST) (No. 2012R1A2A2A01046086) and National Research Foundation of Korea (NRF) grant funded by the Korean Government (MSIP) (No. 2014R1A4A1008140).

References

(1) S. Kang, S. Choi, M. Kang, J. Kim, H. Kim, T. Hyeon, and Y. Sung, *Adv. Mater.,* **20**, 54 (2008).
(2) X. Zong, H. Yan, G. Wu, G. Ma, F. Wen, L. Wang, and C. Li, *J. Am. Chem. Soc.,* **130**, 7176 (2008).
(3) H. J. Donga, G. Chen, J. X. Sun, C. M. Li, Y. G. Yu, and D. H. Chen, *Appl. Catal. B,* **134-135**, 46 (2013).
(4) Q. J. Xiang, J. G. Yu, and M. Jaroniec, *Chem. Soc. Rev.,* **41**, 782 (2012).
(5) S. Ito, K. R. Thampi, P. Comte, P. Liska, and M. Gratzel, *Chem. Commun.,* 268 (2005).
(6) S. J. Doh, C. Kim, S. G. Lee, S. J. Lee, and H. Kim, *J. Hazard. Mater.,* **154**, 118 (2008).
(7) G. Dai, J. Yu, and G. Liu, *J. Phys. Chem. C,* **116**, 15519 (2012).
(8) C. Xu, Y. Liu, B. Huang, H. Li, X. Qin, X. Zhang, and Y. Dai, *Appl. Surf. Sci.,* **257**, 8732 (2011).
(9) G. P. Dai, J. G. Yu, and G. Liu, *J. Phys. Chem. C*, **116**, 15519 (2012).
(10) C. Dong, K. L. Wu, X. W. Wei, X. Z. Li, L. Liu, T. H. Ding, J. Wang, and Y. Ye, *CrystEngComm.,* **16**, 730 (2014).
(11) Y. Song, J. Zhu, H. Xu, C. Wang, Y. Xu, H. Ji, K. Wang, Q. Zhang, and H. Li, *J. Alloys Compd.,* **592**, 258 (2014).
(12) C. Yu, G. Li, S. Kumar, K. Yang, and R. Jin, *R. Adv. Mater.,* **26**, 892 (2014).
(13) C. Feng, G. Li, P. Ren, Y. Wang, X. Huang, and D. Li, *Appl. Catal. B,* **158-159**, 224 (2014).
(14) H. Dong, G. Chen, J. Sun, Y. Feng, C. Li, G. Xiong, and C. Lv, *Dalton Trans.,* **43**, 7282 (2014).
(15) S. Park, J. M. Lee, Y. K. Jo, I. Y. Kim, and S. J. Hwang, *Dalton Trans.*, **43**, 10566 (2014).
(16) G. Panthi, N. A. M. Barakat, K. A. Khalil, A. Yousef, K. S. Jeon, and H. Y. Kim, *Ceram. Int.,* **39**, 1469 (2013).
(17) B. Muktha, G. Madras,T. N. Guru Row, U. Scherf, and S. Patil, *J. Phys. Chem. B,* **111**, 7994 (2007).
(18) D. Meissner, R. Memming, and B. Kastening, *Chem. Phys. Lett.*, **96**, 34 (1983).
(19) G. Panthi, N. A. M. Barakat, S. S. Al-Deyab, M. El-Newehy, D. R. Pandeya, and H. Y. Kim, *J. Appl. Polym. Sci.,* **127**, 2025 (2012).
(20) T. Uyar, A. Balan, L. Toppare, and F. Besenbacher, *Polymer,* **50**, 475 (2009).
(21) Z. Sun, E. Zussman, A. L. Yarin, J. H. Wendorff, and A. Greiner, *Adv. Mater.,* **15**, 1929 (2003).
(22) X. Wang, B. Ding, G. Sun, M. Wang, and J. Yu, *Prog. Mater. Sci.*, **58**, 1173 (2013).
(23) H. Yu, Q. Dong, Z. Jiao, T. Wang, J. Ma, G. Lu, and Y. Bi, *J. Mater. Chem. A,* **2**, 1668 (2014).
(24) L. Ji, A. J. Medford, and X. Zhang, *Polymer,* **50**, 605 (2009).
(25) D. Li and Y. Xia, *Adv. Mater.,* **16**, 1151 (2004).
(26) V. Beachley and X. Wen, *Mater. Sci. Eng. C,* **29**, 663 (2009).
(27) W. Zhang, J. Liu, and G. Wu. *Carbon,* **41**, 2805 (2003).
(28) H. H. Yi, Q. F. Yu, X. L. Tang, P. Ning, L. P. Yang, Z. Q. Ye, and J. H. Song, *Ind. Eng. Chem. Res.,* **50**, 3960 (2011).
(29) J. F. Weaver and G. B. Hoflund, *Chem. Mater.,* **6**, 1693 (1994).
(30) C. W. Xu, Y. Y. Liu, B. B. Huang, H. Li, X. Y. Qin, X. Y. Zhang, and Y. Dai, *Appl. Surf. Sci.,* **257**, 8732 (2011).
(31) J. D. Zhuang, W. X. Dai, Q. F. Tian, Z. H. Li, L.Y. Xie, J. X. Wang, and P. Liu, *Langmuir,* **26**, 9686 (2010).
(32) T. X. Wu, G. M. Liu, and J. C. Zhao, *J. Phys. Chem. B,* **102**, 5845 (1998).